3. SOLUTE TRANSPORT MODELING USING MORPHOLOGICAL PARAMETERS OF STEP-POOL REACHES

Mario A. Jiménez[1] and Ellen Wohl[2]

[1]Universidad Nacional de Colombia – Sede Medellín. Medellín – Colombia

[2]Colorado State University. Colorado – United States

ABTRACT

Step-pool systems have been widely studied during the past few years, resulting in enhanced knowledge of mechanisms for sediment transport, energy dissipation and patterns of self-organization. We use rhodamine tracer data collected in nine step-pool reaches during high, intermediate and low flows to explore scaling of solute transport processes. Using the scaling patterns found, we propose an extension of the Aggregated Dead Zone (ADZ) approach for solute transport modeling based on the morphological features of step-pool units and their corresponding inherent variability within a stream reach. In addition to discharge, the reach-average bankfull width, mean step height, and the ratio of pool length to step-to-step length can be used as explanatory variables for the dispersion process within the studied reaches. These variables appeared to be sufficient for estimating ADZ model parameters and simulating solute transport in predictive mode for applications in reaches lacking tracer data.

Key words: *solute transport, step-pool, fluvial morphology, simulation, ADZ solute transport model*.

3.1 INTRODUCTION

The primary objective of the research described here is to use morphological parameters of step-pool sequences to model solute transport in stream segments for which tracer data are not available. We first review recent work on the formation and morphology of step-pool sequences, and then

review modeling of solute transport processes, before describing the tracer and morphologic data from several step-pool sequences in the Colorado Rocky Mountains, which we use to propose and test a morphologically based model of solute transport in step-pool streams.

Step-pool systems have been widely studied during the past few years, resulting in a broad knowledge regarding mechanisms for sediment transport, energy dissipation and geometrical patterns of self-organization. Such systems occur over a wide range of slopes above 0.02 m/m [*Chin*, 2003; *Wilcox and Wohl*, 2006; *Church and Zimmerman*, 2007], where other morphologic configurations such as cascades can also be found [*Montgomery and Buffington*, 1997]. Step-pool sequences and cascades can be distinguished based on their hydraulic and bedform characteristics, facilitating identification of each channel type from field observations. Moreover, these systems normally occur in the upper areas of a watershed and because of having high transport capacity, they play an important role moving sediments and nutrients downstream, as well as assimilating polluting solutes coming from point or non-point sources, such as those related to agricultural practices or waste water from mining [*Church and Zimmermann, 2007; Turowski et al., 2009; Chin, 2002*].

Alluvial step-pool units consist of relatively immobile cobbles, boulders or instream logs that span the channel width, forming a step followed by a scour pool containing finer sediment (Figure 3-1).

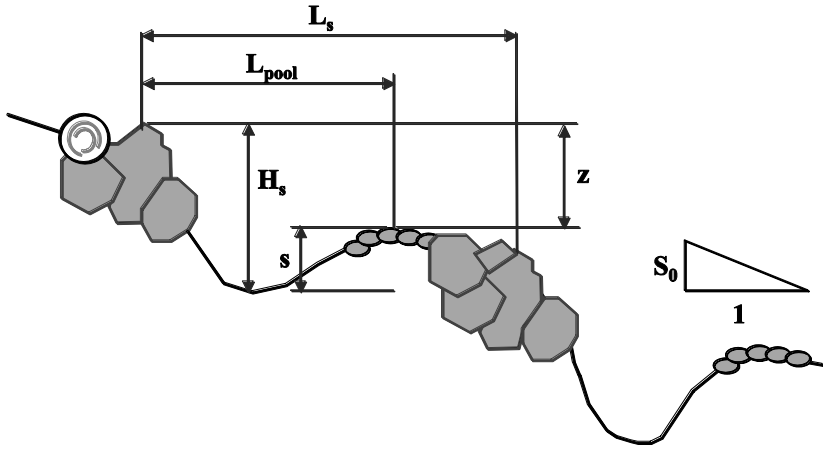

Figure 3-1. Schematic step-pool morphology where H_s, L_s, L_{pool} and S_0 are step height, step to step length, pool length and reach slope respectively. The step-pool unit is also represented by the step to step drop, z.

The geometry of a step-pool unit is described via step length, L_s, and step height, H_s, (Figure 3-1), which influence hydraulic flow regimes and sediment transport processes in step-pool sequences [*Chin and Wohl*, 2005; *Church and Zimmermann*, 2007; *Comiti et al*., 2009]. *Abrahams et al.* [1995] found a strong relationship between L_s, H_s and the channel reach slope, S_0 (equation 3-1), such that $H_s/L_s/S_0$ remains almost constant over a wide range of slopes. More recently, however, *Comiti et al*., [2005] and *Church and Zimmerman* [2007] showed that for idealized step-pool arrangements, *i.e.*, those sequences where steps control nearly all the drop in step-pool channels, step steepness increases with slope. This is expressed in equation (3-2), where $k = L_s/s$ is a nearly constant parameter ranging between 6 and 8, which represents the scoured pool geometry. *Comiti et al.* [2005] proposed an empirical equation (3-3) to explain relations among step-pool geometry features. This model was derived by combining data from natural step-pool units and scour holes downstream of grade-control structures, for which the ideal assumption underlying equation (3-2) is not necessarily satisfied, since the entire step-to-step drop can be influenced by the development of a tread downstream from the scoured hole [*Church and Zimmerman*, 2007].

$$1 \le \frac{H_s / L_s}{S_0} \le 2 \qquad 3\text{-}1$$

$$\frac{H_s / L_s}{S_0} = \frac{kS_0 + 1}{kS_0} \qquad 3\text{-}2$$

$$\frac{H_s}{z} = 0.89\left(\frac{z}{L_s}\right)^{-0.46} \qquad 3\text{-}3$$

In addition to studies highlighting the mutual adjustment between the geometrical features of step-pool units, other studies have examined the internal variability of these features within a reach. In contrast to the regular step spacing suggested by the step-unit geometry given by equations (3-1) to (3), *Curran and Wilcock* [2005] showed that the variability in step spacing along a step-pool channel can be represented through an exponential frequency distribution (equation 4) for those cases where the most significant step-forming process is related to material that gets anchored against keystones or other mechanisms related to forced step-pool units. The proposed distribution for the step spacing x is described by the mean of the distribution, β, and a minimum possible value

given for x_0, also called the exclusion zone, a region immediately downstream from a step where a second step cannot be formed. A more segregated approach was presented by *Myers and Swanson* [1997] for pool-riffle and step-pool sequences, where the pool length is represented with a Gamma distribution using a unique exclusion zone value, and the non-pool length downstream from the pool by a Poisson distribution.

$$f(x) = \frac{1}{\beta} e^{-\frac{1}{\beta}(x - x_0)}; \quad \forall x \geq x_0 \qquad 3\text{-}4$$

The planform variability within step-pool reaches has also received attention in several studies, particularly because it can strongly influence water quality assimilation and physical habitat identification. Bankfull width appears to be an especially useful parameter for describing planform variability, given its direct connection with flow regimes as well as ability to serve as a scale factor when different stream reaches are compared. Besides bedform variability, *Myers and Swanson* [1997] represented width variations along morphological units with a Gamma probability function. *Harman et al.* [2008] proposed a log-normal distribution to explain within-reach width variations, and they represented the reach-average hydraulic geometry parameters more reliably by using the geometric mean of width, depth and velocity, rather than the arithmetic values. *Moody and Troutman* [2002] also found in-channel width variations that followed a marginal log-normal distribution, and they demonstrated the suitability of the approach across several orders of magnitude and different morphologic stream types, including boulder and sand stream beds. In addition, they highlighted the concordance between the statistical behaviors for width and mean depth, and the corresponding hydraulic geometry equations derived from the data set used.

Despite the recent advances in understanding step-pool systems at spatial scales comparable to their morphologic unit size, several questions remain unsolved with respect to solute transport processes, which have received less attention in terms of the linkages with channel morphology features and their spatial variability throughout a stream network. Those aspects become further relevant in the context of environmental management, especially for water quality modeling, to support environmental discharge estimation and stream restoration.

Transient storage models have been widely applied at the reach scale to assess solute transport mechanisms [*Lees et al.*, 1998; *Runkel and Broshears*, 1991; *Lees et al.*, 2000; *Camacho and González*, 2008], hyporheic exchange rates [*Harvey et al.*, 1996; *Choi et al.*, 2000;

Kazezyılmaz-Alhan and Medina Jr, 2006], linkages between channel geometry and hydraulic patterns [*Richardson and Carling*, 2006; *Smith et al.*, 2006; *Wondzell*, 2006], and quantification of habitat abundance [*Lancaster and Hildrew*, 1993; *Lancaster et al*., 1996]. These types of models describe the lumped dispersion processes within a reach by including equivalent stagnant or dead zones that account not only for surface transient storage, but also for storage in the hyporheic zone.

The Transient Storage model (TS) [*Bencala and Walters*, 1983] and the Aggregated Dead Zone (ADZ) model [*Beer and Young*, 1983] have provided a basis for important research in solute transport, as well as for engineering applications in the last two decades.

For the ADZ framework, the transport process within a reach is conceptualized to occur within two regions. The solute first enters a completely active zone, where pure advection takes place for a time span, τ. The solute is then transported and enters a completely stirred aggregated dead zone, where dispersion takes place during a remaining hydraulic residence time given by T_r (Figure 3-2). The mean passage time of the solute along the stream reach is then given by $t_m = \tau + T_r$. The mass balance equation for the ADZ model under steady flow conditions is given by equation (3-5), where C_u denotes the known input concentration at the upstream edge of the reach and $C(t)$ the downstream output concentration [*Lees et al.*, 2000].

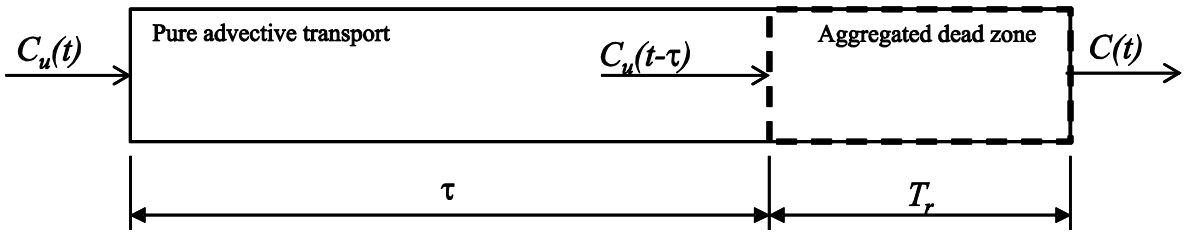

Figure 3-2. Conceptual representation of the solute mixing process along a stream reach using the ADZ model. The left area represents the zone where the solute does not suffer dispersion during a time τ, so that $C_u(t) = C_u(t-\tau)$. The right area represents the aggregated dead zone where the solute is completely mixed during a time T_r thus producing an output concentration $C(t)$.

$$\frac{dC(t)}{dt} = \frac{1}{t_m - \tau}\left[C_u(t-\tau) - C(t)\right] \qquad 3\text{-}5$$

An important assumption of the ADZ model is that only a fraction of the total water volume within the reach is completely stirred: this proportion is identified as the dispersive fraction, *DF*, as shown in equation (3-6). It is worth noting that *DF* can be expressed in terms of either the ratio of

the well mixed volume, V, to the total reach volume, V_{TOTAL}, or, under steady flow conditions and discharge Q, the ratio between the corresponding resident times for both volumes. DF can vary from 0, which represents a completely advective system, to 1, representing an ideal dispersive system.

$$DF = \frac{V}{V_{TOTAL}} = \frac{T_r Q}{t_m Q} = \frac{T_r}{t_m} = \frac{t_m - \tau}{t_m} = 1 - \frac{\tau}{t_m} \qquad 3\text{-}6$$

An initial finding regarding DF was that it is nearly constant for a wide range of discharges [*Wallis et al.*, 1989]. This assumption continues to be used to support some ADZ applications, especially in flat regions because the assumption implies only measuring or estimating the mean travel time along the reach of interest. Nevertheless, *González* [2008] found that DF could vary up to 22% within the same reach in mountain streams under different flow conditions. Hence, the dispersion process along a mountain stream reach should not be assessed by carrying out a single or a few tracer experiments. Besides, economic limitations typically make DF, t_m or τ, infeasible to obtain by tracer measurements throughout an entire mountainous region or watershed.

Because of the good performance reported for the ADZ approach for modeling solute transport, as well as the fact that the model is known for having physically based and measurable parameters and for being parsimonious (two parameters), we adopt it to explore scaling patterns of solute transport processes in step-pool sequences. The more recent knowledge available for such systems allows us to explore a morphologically based representation of the model with the hope that it can be used to support solute transport applications in ungaged regions, as well as habitat abundance assessment and distributed hydrologic modeling.

In the subsequent sections we first describe de ADZ model framework and how it was used to obtain solute transport parameters for nine step-pool reaches during high, intermediate and low flows. We then derived morphologic features for those reaches using detailed topographic data and applying an objective method. Next, transport parameters and morphologic parameters are combined base on dimensionless forms for discharge, travel times and features of morphological step-pool-run units, providing evidences to support the invariance of the solute movement mechanisms. Finally, we present a morphologic-based extension for the ADZ model that we test with the available data.

3.2 FIELD AREA AND DATA SET

Recent studies of flow resistance [*David et al*., 2010a] and at-a-station hydraulic geometry [*David et al.*, 2010b] in steep streams are based on information collected from the Fool Creek (FC) and East St. Louis Creek (ESL) watersheds in the Fraser Experimental Forest in the Colorado Rocky Mountains, United States (Figure 3-3). We used data from 9 step-pool reaches from these creeks.

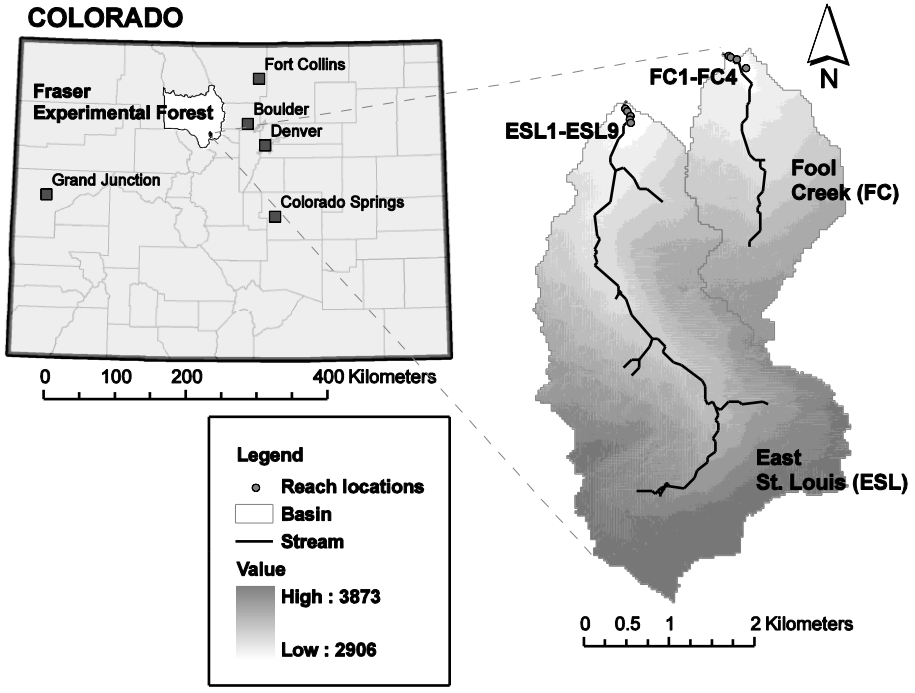

Figure 3-3. Location map of the studied step-pool reaches

The FC basin at the study site drains 2.9 km^2 and includes four surveyed step-pool reaches. The ESL watershed at the study site drains 8.7 km^2 and includes five measured step-pool reaches. Both FC and ESL are influenced by large amounts of instream wood, and most of the steps include not only boulders but also wood jams. Steps formed by in-stream wood are dominant in reaches ESL2 and FC3. ESL4 and FC1 are the only step-pool reaches where all of the steps are boulder steps [*David et al*., 2010a].

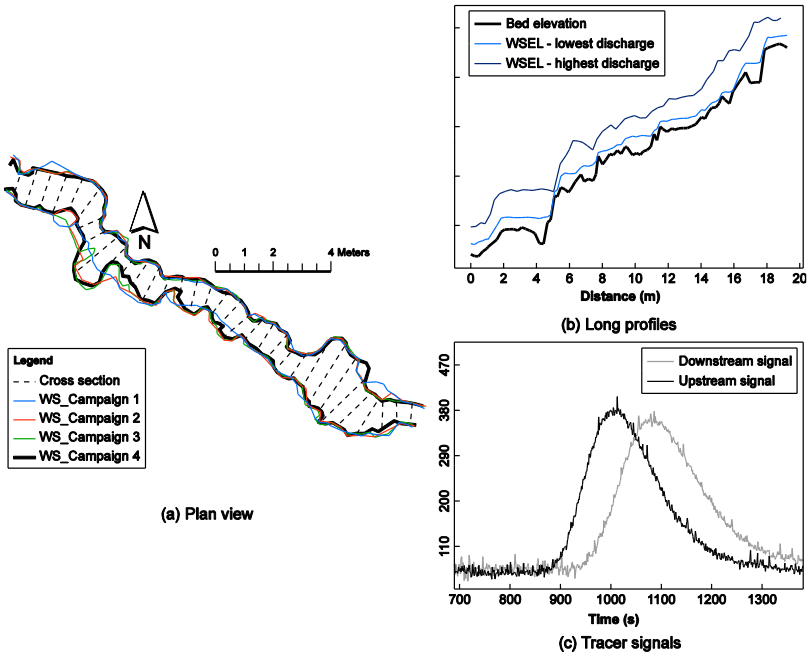

Figure 3-4. Data set for reach FC4 as an example of the type of data available; (a) plan view; (b) longitudinal profile; and (c) tracer data.

David et al. [2010a] describe the set of data collected for within-bank flow stages covering high, intermediate and low flow conditions for all reaches. For each of those stages, water surface and bed elevation along the thalweg and banks were profiled at 15 cm intervals using a laser theodolite, which allowed subsequent calculation of average slope value as well as application of objective methods to quantify the geometrical features of step-pool units for each reach. Together with the theodolite data, ground-based LiDAR (Light Detection and Ranging) scans were carried out to capture bank and bed topography during the lowest flow period. The LiDAR data was merged with the theodolite surveys in order to generate cross sections spaced at 1-m intervals for each flow condition. Hydraulic variables including width, flow depth, hydraulic radius and cross sectional area were derived using the cross-sectional data.

Figure 3-4 illustrates the set of information provided by *David et al*. [2010a] for the FC4 reach as an example of the data available, and Table 3-1 shows the mean geometric and hydraulic features for all reaches.

Table 3-1. Hydraulic and morphologic attributes for the available reaches, from [*David et al.*, 2010a][a]

Reach	Campaign	Q (m^3/s)	L_r (m)	S_0 (m/m)	W (m)	XS Area (m^2)	H_s (m)	L_s (m)	D_{50} (m)	D_{84} (m)
ESL1	1	0.66	29.37	0.093	2.92	0.990	0.63	4.64	0.05	0.16
ESL1	2	0.29	27.30	0.104	2.60	0.700	0.76	4.31	0.05	0.16
ESL1	4	0.06	31.57	0.086	2.01	0.290	0.62	4.97	0.05	0.16
ESL2	1	0.63	13.70	0.093	3.21	1.000	0.52	2.56	0.01	0.07
ESL2	2	0.44	13.99	0.089	2.97	0.740	0.44	2.75	0.01	0.07
ESL2	3	0.31	13.95	0.095	2.86	0.680	0.35	2.58	0.01	0.07
ESL2	4	0.11	14.04	0.092	2.57	0.450	0.46	2.78	0.01	0.07
ESL4	1	0.68	15.57	0.128	2.86	0.990	0.53	2.22	0.07	0.17
ESL4	2	0.40	16.31	0.110	2.69	0.780	0.60	2.64	0.07	0.17
ESL4	3	0.26	15.75	0.121	2.48	0.570	0.55	2.87	0.07	0.17
ESL4	4	0.16	16.54	0.102	2.32	0.500	0.47	2.49	0.07	0.17
ESL8	1	0.57	30.68	0.099	3.16	0.910	0.39	4.50	0.07	0.17
ESL8	2	0.43	32.65	0.086	3.03	0.780	0.42	4.58	0.07	0.17
ESL8	3	0.27	31.38	0.091	2.73	0.590	0.41	4.48	0.07	0.17
ESL8	4	0.17	35.48	0.082	2.58	0.480	0.43	5.87	0.07	0.17
ESL9	1	0.57	16.26	0.115	2.79	0.920	0.44	2.62	0.06	0.15
ESL9	2	0.33	16.51	0.111	2.62	0.720	0.43	2.69	0.06	0.15
ESL9	3	0.27	16.22	0.117	2.53	0.640	0.46	2.59	0.06	0.15
ESL9	4	0.16	18.64	0.095	2.28	0.470	0.44	3.08	0.06	0.15
FC1	1	0.33	23.12	0.062	1.97	0.380	0.20	2.78	0.03	0.08
FC1	2	0.05	23.20	0.060	1.57	0.170	0.20	3.22	0.03	0.08
FC1	3	0.08	23.74	0.060	1.63	0.180	0.19	2.83	0.03	0.08
FC1	4	0.02	25.12	0.058	1.28	0.090	0.19	2.42	0.03	0.08
FC2	1	0.26	14.38	0.074	1.63	0.390	0.25	2.30	0.03	0.08
FC2	2	0.05	14.18	0.077	1.41	0.200	0.22	2.44	0.03	0.08
FC2	3	0.07	15.05	0.073	1.41	0.170	0.19	3.01	0.03	0.08
FC2	4	0.01	14.93	0.071	1.13	0.080	0.20	2.72	0.03	0.08
FC3	1	0.24	13.48	0.093	2.12	0.550	0.36	2.51	0.01	0.05
FC3	2	0.04	12.22	0.092	1.66	0.240	0.29	2.44	0.01	0.05
FC3	3	0.06	14.87	0.079	1.64	0.230	0.33	3.55	0.01	0.05
FC3	4	0.01	11.90	0.095	1.36	0.120	0.32	2.92	0.01	0.05
FC4	1	0.37	18.86	0.141	1.65	0.490	0.49	2.87	0.05	0.10
FC4	2	0.06	19.82	0.130	1.39	0.210	0.42	3.63	0.05	0.10
FC4	3	0.06	19.01	0.136	1.45	0.230	0.49	2.97	0.05	0.10
FC4	4	0.02	19.23	0.132	1.25	0.140	0.38	3.01	0.05	0.10

[a]Abbreviations correspond to discharge, Q, reach length, L_r, reach slope, S_0, mean top width, W, cross sectional areal, XS Area, mean step height, H_s, average step-to-step length, L_s, and particle sizes D_{50} and D_{84}.

Tracer experiments using Rhodamine WT were performed to estimate characteristic solute travel times and longitudinal dispersion mechanisms. Fluorometers were placed at the upstream and

downstream edges of a reach to measure the tracer cloud passage for a sufficient time interval to ensure that the registered base concentration level in the stream was recovered. Measurements were repeated four times for each flow condition.

3.3 METHODS

3.3.1 Solute transport model

The ADZ fundamental equation (3-5) can be expressed in the form of equation (3-7) in order to seek an analytical solution for the downstream concentration *C(t)*.

$$\int_{t_0}^{t} \frac{dC(t)}{C_u(t-\tau)-C(t)} = \int_{t_0}^{t} \frac{dt}{T_r} \qquad 3\text{-}7$$

However, since $C_u(t-\tau)$ is also time-dependent, an approach to the analytical solution of (7) can be obtained by making the period $\Delta t = t-t_0$ short enough that $C_u(t-\tau)$ can be considered as a constant in the integral. This assumption yields equation (3-8), which is usually expressed in the form of equation (3-9), corresponding to the discrete-time form of the ADZ model [*Wallis et. al*, 1989; *Camacho*, 2000; *Richardson and Carling*, 2006; *González*, 2008], where δ is the time delay, τ, expressed as integer time steps, and $c_{(k)}$ is the solute concentration at the *k*-th sample time interval.

$$C(t) = \left(1-e^{-\Delta t/T_r}\right) C_u(t_0-t) + C(t_0)e^{-\Delta t/T_r} \qquad 3\text{-}8$$

$$c_{(k)} = Bc_{u(k-\delta)} - Ac_{(k-1)}; \quad A = -e^{-\Delta t/T_r}; \quad B = 1+A; \quad \delta = \tau/\Delta t \qquad 3\text{-}9$$

Predictions using equation (3-9) depend on definition of the physical parameters τ and $T_r=t_m-\tau$, the boundary upstream condition c_u and the user-defined discretization interval Δt.

3.3.2 Tracer signal processing

Some of the available tracer signals are shown in Figure 3-5 to illustrate the set of typical interferences obtained during the tracer experiments. Interferences include high noise for some of the measured signals while preserving the expected response (Figure 3-5a), differences in the base concentration level registered upstream and downstream (Figure 3-5b), and losses of information

either because of abrupt concentration changes or because the sampling time was insufficient to measure the total breakthrough curve.

To overcome such situations, the original tracer signals (upstream and downstream from the reach) were first filtered using a multiple pass median filter with a window size varying from 3 to 24 seconds, depending on the signal noise. Once filtered, the resultants signals were truncated by defining a concentration threshold above their corresponding base concentration values, equivalent to 10% of the measured concentration range. At this point, the backward and forward tails of the signal were isolated in order to calculate a mean base concentration upstream and downstream whose difference was used to adjust both signals at the same level. Moreover, the first arrival time, τ, and the mean travel time, t_m (measured to the center of mass), of the truncated area were then assessed for both signals. In this way, the differences between the corresponding times for the upstream and downstream filtered signals correspond to a first approach to the first arrival time and mean travel time values within the reach.

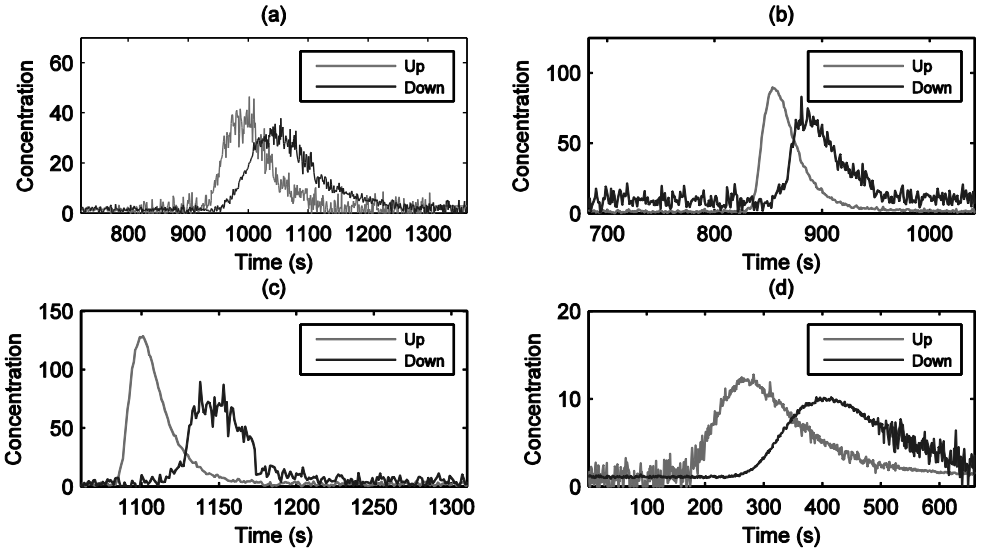

Figure 3-5. Type of interferences found in some of the tracer signals

Once the signals were adjusted to the same base concentration level, Monte Carlo simulations (N = 5000) were performed in order to obtain the pair (τ, t_m) around the initial values previously estimated, which best fit the downstream signal using the discrete-time ADZ approach. Figure 3-6 shows results from this method for those cases in Figure 3-5. It worth noticing that even when it

was not possible to capture the entire passage time downstream, it was possible to get information from the registered signals in order to characterize the dispersive processes.

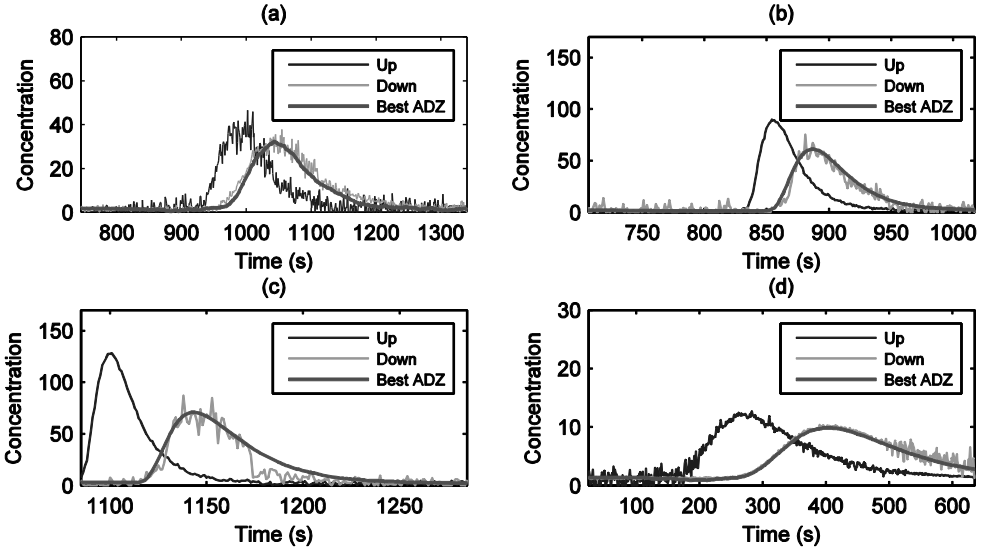

Figure 3-6. Best ADZ simulation fitted to the observed tracer signal after standardizing to the same base concentration level.

3.3.3 Bankfull stage

Bankfull stage has been widely related to the hydrologic condition that performs most geomorphic work. This implies that discharges reaching bankfull stage are responsible for several geometric signatures along a specific stream reach. The channel width at bankfull stage, W_B, is likely to be one of the more significant variables to measure in the field, and has been reported as a scale parameter for the estimation of bankfull discharges and geometric features for both lowland and upland streams. *Chin* [1999] showed that step-pool spacing could be expressed as units of channel width, which resemble the rhythmic patterns of pool-riffle sequences. The strong relation between W_B and the watershed area at the basin scale, when the area is used as a surrogate for discharge, is also well known [*Leopold*, 1994; *Knighton, 1998; Vianello and D'Agostino*, 2007]. Hence, we adopted W_B as a scale parameter, which facilitates future applications to other catchments of the approach described here.

Bankfull width was calculated for each reach as the average of the individual cross sectional values obtained for the stage which maximizes the specific stream power $\omega = \gamma Q S_0 / W$. To estimate Q at different stages, the Manning equation was applied, with the Manning's n coefficient taken as

the mean value obtained using the mean velocity calculated from the tracer experiments and the corresponding stream-flow geometry. We found that this method yields comparable results to those obtained when bankfull stage is defined as the water surface elevation at which the width-to-depth ratio becomes a minimum [*Radecki-Pawlik*, 2002]. Table 3-2 shows the average W_B for all the available reaches compared with the mean width values, W, corresponding to the highest measured discharge.

Table 3-2. Average bankfull width

Reach	W_B (m)	W (m)	Relative deviation (%)
ESL1	2.98	2.92	2.0
ESL2	3.72	3.21	13.6
ESL4	2.96	2.86	3.4
ESL8	3.10	3.16	-2.1
ESL9	3.42	2.79	18.4
FC1	2.56	1.97	23.2
FC2	1.78	1.63	8.4
FC3	2.03	2.12	-4.6
FC4	1.66	1.59	4.1

3.3.4 Morphologic features

Several morphologic characteristics were objectively defined so that we could explore their influence on the transport parameters derived in connection with the ADZ model. We defined step-pool units along the bed profile using the method proposed by *Zimmermann et al*. [2008], which is based on the identification of key signatures along the bed profile normalized by the mean bankfull width (W_B). The method is thus considered scale-free and applicable to any step-pool channel.

Average values for the step-to-step length (L_s), pool length (L_{pool}) and step height (H_s) were subsequently derived from the step-pool units identified along each reach. Table 3-3 summarizes the number of step-pool units derived, as well as the mean morphological values calculated. Figure 3-7 shows the expected L_s and L_{pool} dependency on the bankfull width, with a stronger relationship for L_{pool}. We analyzed the variability of the dimensionless variables L_{pool}/W_B and L_s/W_B in order to make all the observations comparable. In this context, Figure 3-7 also displays the histogram of step length values sampled from all longitudinal profiles, after being normalized using W_B. The distribution agrees with previous analyses of step-pool profiles by indicating that step-pool spacing typically ranges from less than one to around four channel widths [*Chin, 1999; Chin and*

Wohl, 2005]. The L_s/W_B histogram also indicates that there is more than one mode, with the higher frequency corresponding to that for the L_{pool}/W_B histogram.

Table 3-3. Number of step-pool units identified and their mean features following *Zimmermann et al.* [2008][a]

Reach	Campaign 1	Campaign 2	Campaign 3	Campaign 4	[a]L_s (m)	[b]L_{pool} (m)	[c]H_s (m)
ESL1	6	5	0	5	5.62	3.22	0.53
ESL2	4	2	2	2	3.82	2.97	0.50
ESL4	3	4	5	5	3.48	2.15	0.44
ESL8	8	6	7	3	4.45	2.18	0.32
ESL9	3	2	4	3	4.25	2.39	0.40
FC1	1	0	4	3	4.24	1.85	0.21
FC2	4	2	3	2	3.13	1.39	0.16
FC3	4	3	1	1	2.32	1.76	0.29
FC4	7	5	6	7	2.51	1.37	0.25

[a] [b] [c]Mean calculated values for L_s, L_{pool}, and H_s using the objective method by Zimmermann el al. [2008]. The corresponding field values are reported in Table 3-1.

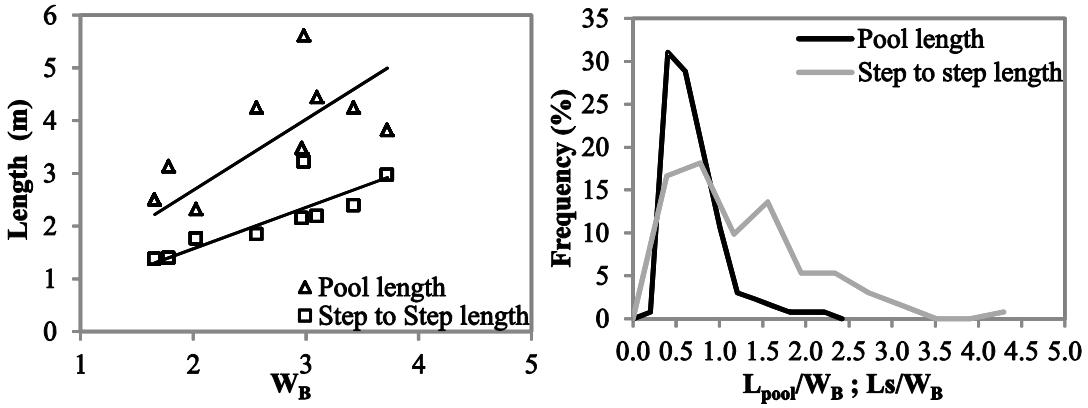

Figure 3-7. Relation of characteristic lengths with reach-average width (left), and normalized frequency histograms for L_{pool} and L_s (right)

To assess the influence on dispersion coming from the stream planform variability, we quantified the coefficient of variation of the water surface top width (*CVw)* for each discharge. Transects perpendicular to the primary flow direction were created using a set of Visual Basic Macros developed for AutoCAD.

3.3.5 Searching for invariance

In order to facilitate comparison of the solute transport and morphological data, we introduced dimensionless unit discharge, q^* (equation 3-10), and dimensionless travel time, t^*, (given by

equation 3-11 for either t_m or τ) following *Comiti et al.* [2007] and *Ferguson* [2007]. t^* and τ^* can be seen as the inverse of the non-dimensional mean velocity, U^*, and maximum velocity, U^*_{max}, respectively. We also propose including the reach-average bankfull width, W_B, in the normalization strategy because such a variable appears to be easier to estimate either directly in the field or from aerial photos, or by using downstream hydraulic geometry equations [*Leopold*, 1994; *Dodov and Foufoula-Georgiou*, 2004; *Wohl*, 2004; *Vianello and D'Agostino*, 2007]. Similarly, we explored inclusion of the average step height H_s as the roughness scale in equations (3-10) and (3-11) instead of D_{84}, given the differences in the step-forming processes among reaches and the material composing steps.

$$q^* = \frac{Q}{W\sqrt{gD_{84}^3}} \qquad 3\text{-}10$$

$$t^* = \frac{\sqrt{gD_{84}}}{U} = \frac{t\sqrt{gD_{84}}}{L_r} = \frac{1}{U^*} \qquad 3\text{-}11$$

3.4 RESULTS AND DISCUSSION

3.4.1 ADZ model parameters

When power-law functions were derived from the set of non-dimensional pairs (q^*, t^*_m) and (q^*, τ^*), we found high correlation values even when the combined set of data includes information coming from reaches at different watersheds and with different step-forming processes. Figure 3-8(a) and 8(b) displays results obtained using W and D_{84} in the normalization procedures. These plots indicate data segregation between reaches with steps composed completely of wood and steps composed completely of boulders. This pattern becomes clearer for the mean travel time t^*_m. After doing the proposed normalization replacements (W with W_B and D_{84} for H_s), we found an improvement in the q^*-t^*_m (for τ^* it remained almost the same), as well as the best agreement of data within a single tendency (Figure 3-8c and 8d).

In contrast with travel times, when the power law functions were combined following equation (3-6), the dispersive fraction becomes a nearly constant and discharge-independent value, $DF \approx 0.41$ (Figure 3-9a). This invariance arises as a consequence of the strong linear relation between the t_m and τ (Figure 3-9b), a finding previously reported for different stream settings including river

bends, uniform channels and high-gradient streams [*Xia, 1997*; *González, 2008*]. Complementary evidence that *DF* does not change significantly with discharge can be noticed in Figure 3-10 as narrow boxes for every reach.

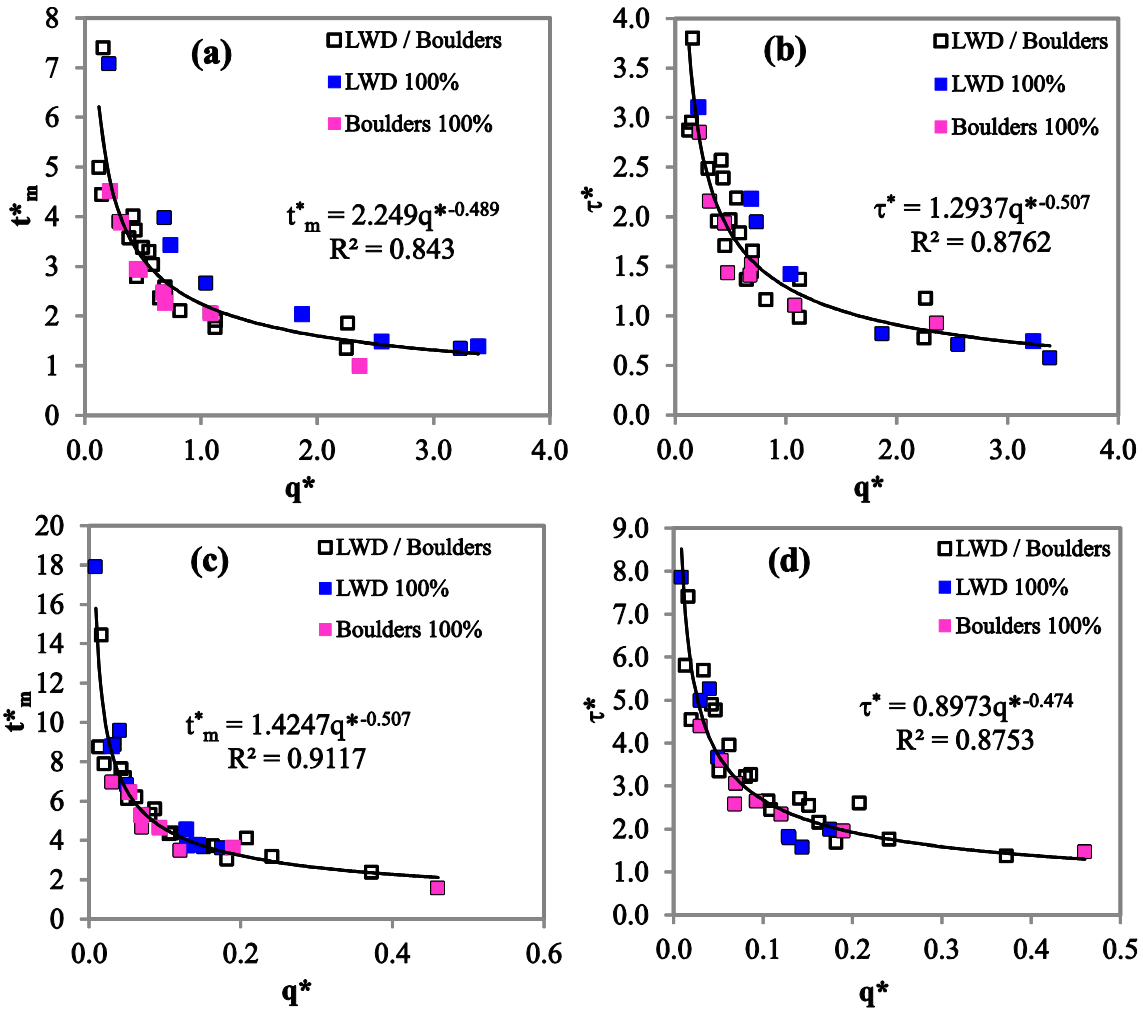

Figure 3-8. Nondimensional travel times relations with discharge q*. (a) and (b) are normalizations using D84 and W. For (c) and (d), *Hs* and W_B were used

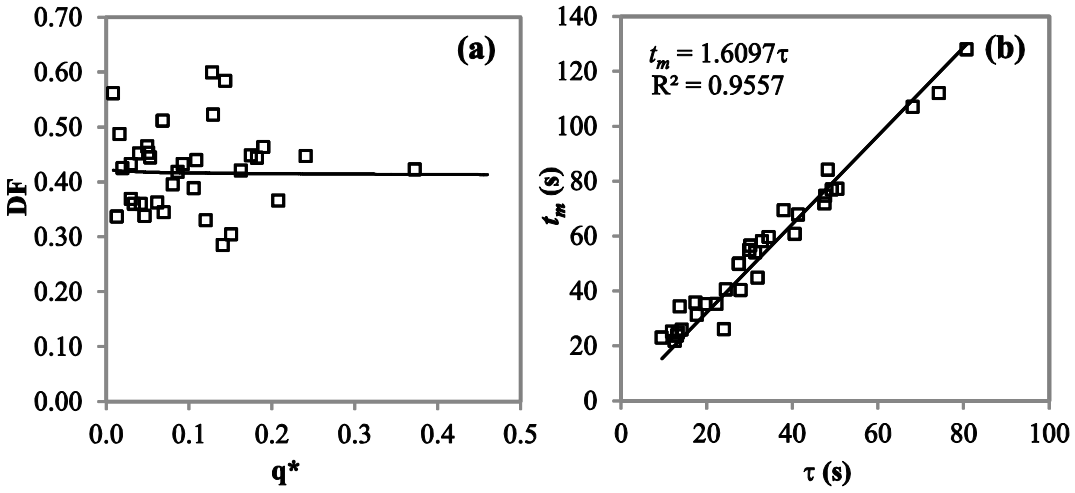

Figure 3-9. Invariance of the dispersive fraction with discharge (a) as a consequence of the strong linearity between t_m and τ (b).

The variability of *DF* among reaches is greater than variability within a reach. Reach-average *DF* values range from 0.36 for ESL1 to 0.57 for ESL2. In order to explain such variability in relation to stream morphological features, we used the coefficient of variation of the water surface top width (*CVw*) and the characteristic lengths L_s and L_{pool} for correlation analysis with the mean values of *DF*.

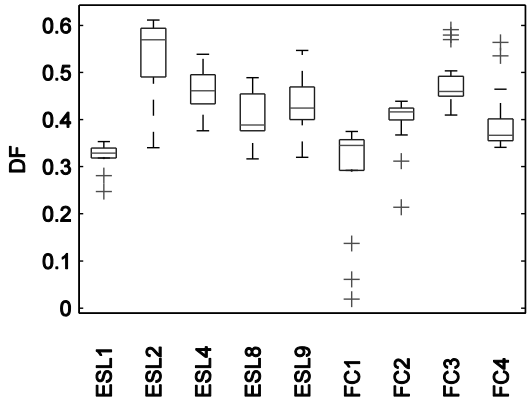

Figure 3-10. Observed variability of dispersive fraction among reaches and within the same reach

We found a clear trend between the averages of *DF* and the L_{pool} to L_s ratio (Figure 3-11), a simple but consistent result taking into account what *DF* means regarding water volumes according to equation (3-6). Thus, a step-pool-run can be seen as a morphological unit whose dispersive characteristics resemble the conceptual ADZ formulation (Figure 3-2), so that the entire dispersion along a reach can be conceptualized as a series of those morphological units having a dispersive

fraction explained partially with the L_{pool}/L_s ratio and characteristic travel times explained in terms of the nondimensional discharge q^*.

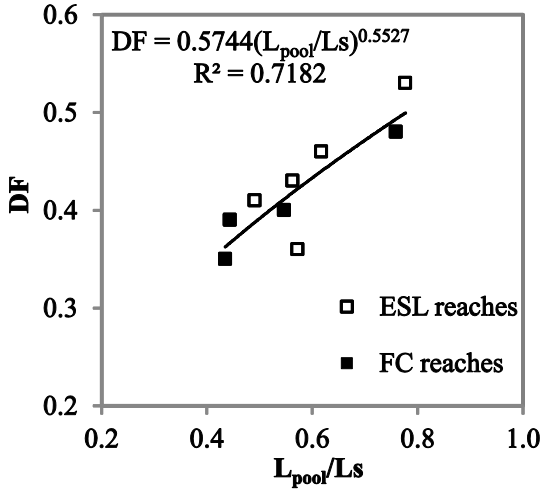

Figure 3-11. Explanation of the dispersive fraction variability in terms of the average (L_{pool}/L_s) parameter

In contrast, a weak trend exists between *DF* and *CVw* (Figure 3-12), which suggests that the higher the variability of *W,* the higher the time of retention in dead zones areas. This relates to the decreasing trend of the *CVw* when plotted against the non-dimensional discharge q^*, indicating a greater effect on dispersion for lower discharges. An underlying explanation was provided by *Zhang and Boufadel* [2010] through the evaluation of pool effects on dispersion, in terms of the nondimensional group $\varepsilon = Q/DW$, where *D* is the transversal dispersion coefficient. When ε reaches low values, the width of the pool becomes important because the transverse dispersive transport within the pool becomes comparable with the convective transport downstream. This condition can be expected when the *CVw* becomes high (low discharge), considering that flow width in steps and runs tends to be lower than in pools, thus creating more interaction of the solute with the pool volume. Conversely, for high discharges (low *CVw*), water which enters a pool spans the whole channel width, causing a well-mixed flow and more convective transport downstream.

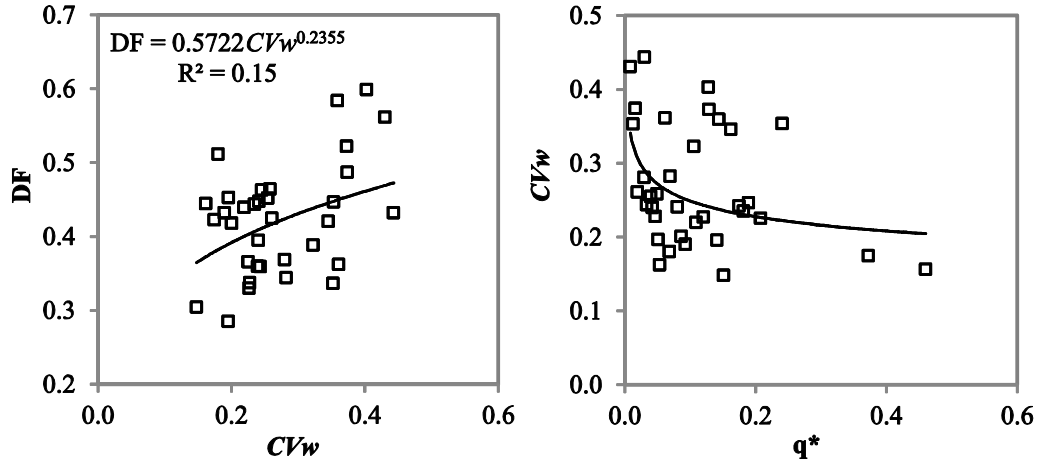

Figure 3-12. Explored correlation between the dispersive fraction and the coefficient of variation of the top width flow

Based on the above discussion, the empirical approach given in Figure 3-11 is proposed to estimate the mean dispersive fraction along a step-pool reach. Deviations from such a center value should be explained in terms of transversal dispersion within a pool, but we are aware that even when the coefficient of variation provides insights into such local processes, further analysis is required. The empirical approach neither account for sources of uncertainty regarding the complete geometrical variability within a specific stream reach or hyporheic solute exchange.

3.4.2 Morphologic invariace

Even when the findings regarding the variability of *DF* appear to be useful to quantify dispersion at different spatial scales, detailed geometrical surveys are needed to assess the explanatory variables H_s, L_s and L_{pool}. Hence, rather than considering the deterministic contributions given by the empirical equation for *DF* and the relations t^*_m-q^* and τ^*-q^*, we assessed the statistical behavior of L_{pool} and the length of the downstream run (L_s-L_{pool}).

A modified exponential probability distribution function (*pdf*) for equation (3-4) was adopted to represent the length of both pools and runs within a reach. An assumption is that the primary step-forming mechanisms are bed roughening and exhumation [*Curran and Wilcock*, 2005; *Curran*, 2007; *Church and Zimmermann*, 2007]. Moreover, the wide scatter between L_{pool} and (L_s-L_{pool}) shown in Figure 3-13 does not suggest interdependence among such variables, thus allowing their statistical treatment independently.

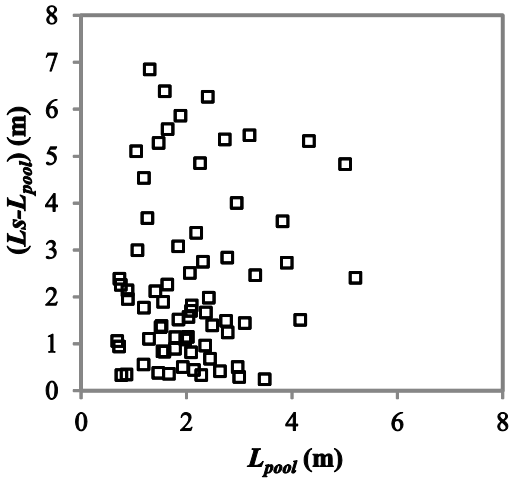

Figure 3-13. Scatter found between pool lengths and their corresponding downstream run lengths

Parameters of the distribution, i.e., the exhumation zone, x_0, and mean value, β, were expressed in terms of a constant ratio to the reach-average bankfull width, a and b, respectively, as shown in equation (3-12). For runs, the constant a equals zero. The fit of each exponential *pdf* was tested using a χ^2 goodness-of-fit (0.1 significance level). It can be noted that in addition to the estimated *pdf* parameters the observed *p*-values are also reported in Table 3-4, which are both higher than the significance level of the test.

$$f(x) = \frac{1}{bW_B} e^{-\frac{1}{bW_B}(x - aW_B)} \qquad 3\text{-}12$$

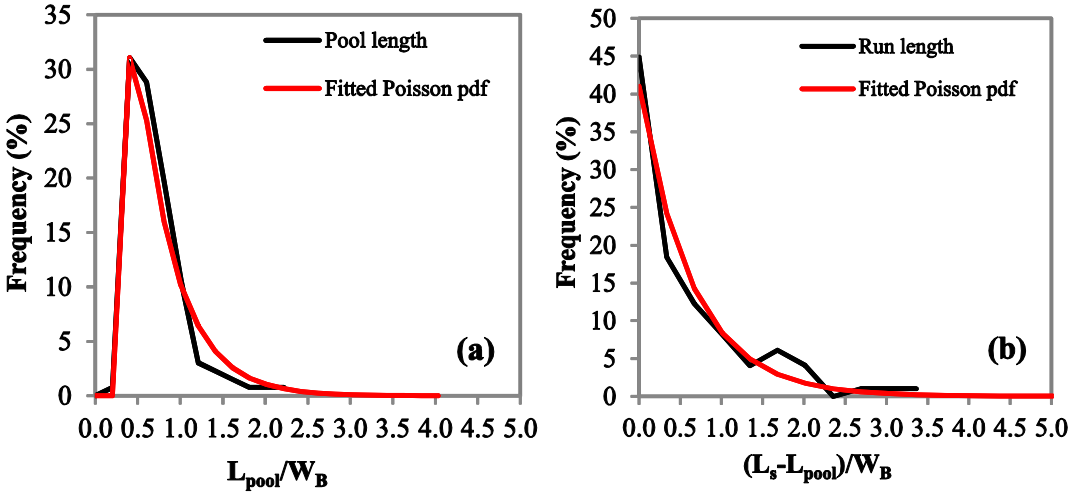

Figure 3-14. Dimensionless probability distribution functions for (a) pool length, and (b) step to step length

Table 3-4. Exponential distribution parameters (β, x_0) estimated by the method of moments

Reach	β	x_0	p-value
Length of pools	0.441	0.441	0.805
Length of runs	0.637	0.000	0.147

3.4.3 Morphologically based scheme

A summary of the analyses described to this point can be used to propose a morphologically based approach for simulating solute transport along step-pool reaches. Assume that the morphologic variables S_0, L_r, W_B and the hydrologic variable Q are known for a specific stream reach (*STEP 1*). Their selection as input data is justified because, for watershed management applications, there are several indirect alternatives to obtain such variables.

Knowing the reach-average bankfull width, the probabilistic behavior of pools and runs can be assessed with two independent exponential *pdf* (*STEP 2*). Thus, it is possible to span the total reach length with a set of random step-pool-run units. At this point, the empirical evidence presented by *Comiti et al.* [2005] was included in order to estimate the corresponding step height H_s for each generated pool length (*STEP 3*). Comparisons with the corresponding values estimated with both the objective method implemented here and the mean field estimations are shown in Figure 3-15. Equation (3-3) yields higher H_s values, whereas most of our data (observed at field and estimated) fall nearly outside the confidence bounds estimated from the empirical model.

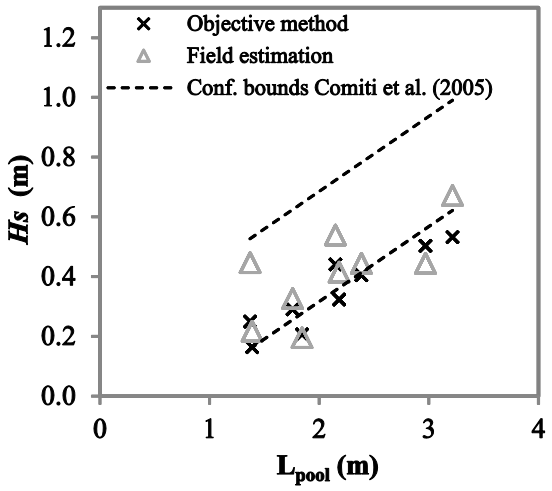

Figure 3-15. Comparisons between the Hs values obtained in this study and estimations made using the empirical equation by *Comiti et al*. [2005]

Confidence bounds were inferred by assuming that the total variance of our data equals the variability of Comiti's original data set. We suggest the implementation of such relations because *Comiti et al.* [2005] had a much larger dataset that also included different formative processes of pools.

The step-pool sequence resulting from *STEP 3* is then characterized with the average values H_s' and (L_{pool}/L_{step})' (the single quotation was introduced to make reference to simulated values), which in turn allow estimating the dispersive fraction and either t^*_m or τ^* from the fitted dimensionless forms given in Figure 3-8 (*STEP 4*). Finally, if an input concentration signal is known upstream from the reach, the discrete ADZ model can be applied with the transport parameters derived (*STEP 5*). Figure 3-16 illustrates the strategy described. Again, Monte Carlo simulations were used to generate N = 5000 step-pool-run random sequences in order to infer the uncertainty associated with the proposed framework due to all the individual contributions coming from the empirical approaches derived and implemented here, and the randomness of the morphological settings along a reach. It is worth mentioning again the uncertainty resulting from the influence that pool width can exert on the dispersion process, as well as the linkages between pool width and discharge.

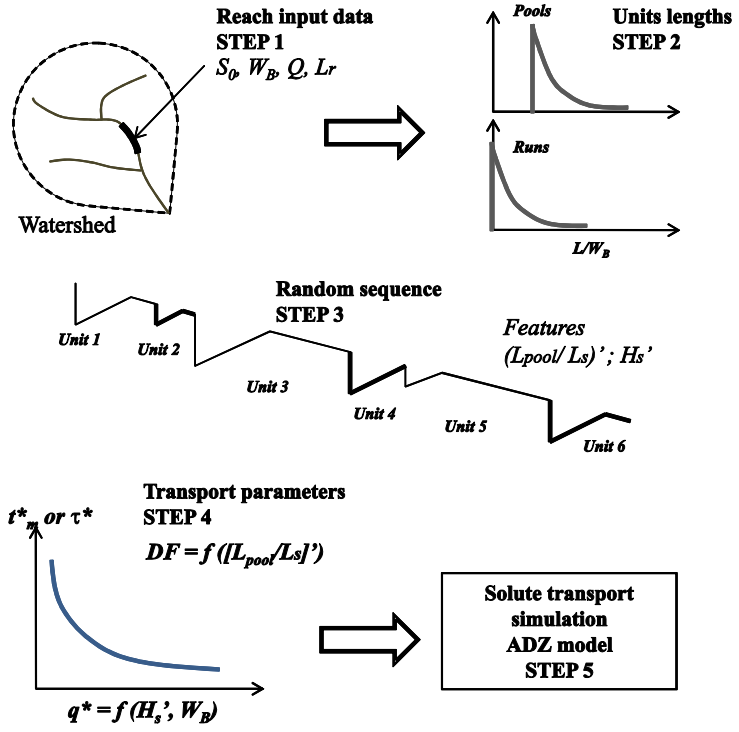

Figure 3-16. Schematic illustration for the proposed morphological framework for modeling solute transport

For the available data from each set of measurements, we assessed the model performance in terms of the Nash efficiency coefficient given by equation (3-13). Higher *E(%)* values indicate a better model performance. C_j corresponds to the fifty percent quantile for the simulated values at each time step j, $C_{o,j}$ is the measured downstream concentration for the time step j and $\overline{C_o}$ is the mean of the downstream measured signal.

$$E = 100\left[1 - \frac{\sum_{j=1}^{T}\left(\sqrt{C_j} - \sqrt{C_{o,j}}\right)^2}{\sum_{j=1}^{T}\left(\sqrt{C_{o,j}} - \sqrt{\overline{C_o}}\right)^2}\right] \qquad 3\text{-}13$$

Table 3-5 summarizes the performance of the model, including as uncertainty sources those corresponding to the probabilistic behavior of L_{pool} and L_s, and errors coming from the application of the relationships DF - (L_{pool}/L_s) and t^*_m - q^* (τ was inferred using equation 3-6).

Table 3-5. Morphologic-based ADZ model performance

Reach	Campaign 1	Campaign 2	Campaign 3	Campaign 4
ESL1	72.4	-	-	75.8
ESL2	95.4	84.6	97.2	98.2
ESL4	99.0	96.5	97.9	94.8
ESL8	91.4	94.9	92.7	93.6
ESL9	87.2	82.3	80.2	96.2
FC1	-	71.2	65.5	87.3
FC2	-	99.5	-	59.7
FC3	94.2	99.4	99.3	95.6
FC4	-	95.5	97.5	79.6

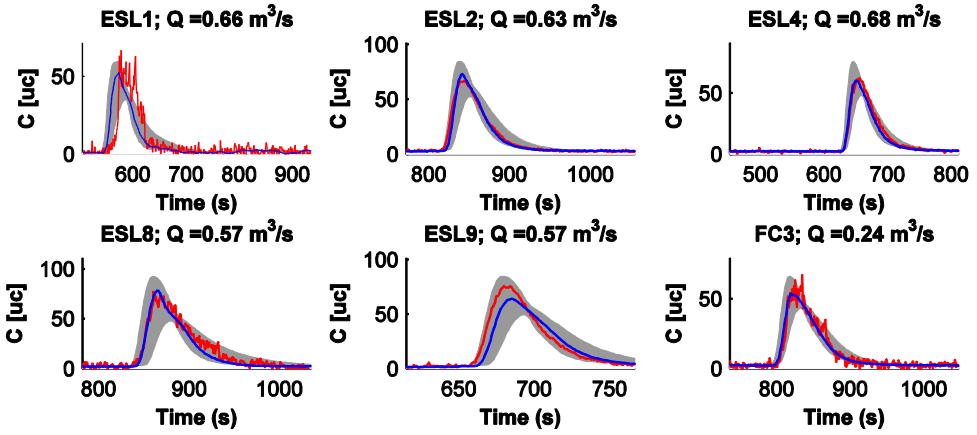

Figure 3-17. Simulated values for flow condition corresponding to campaign No 1. Red and blue lines are the observed and mean simulated breakthrough curves, respectively. The shaded area is limited by the 95th percentile and 5th percentile of predictive distributions.

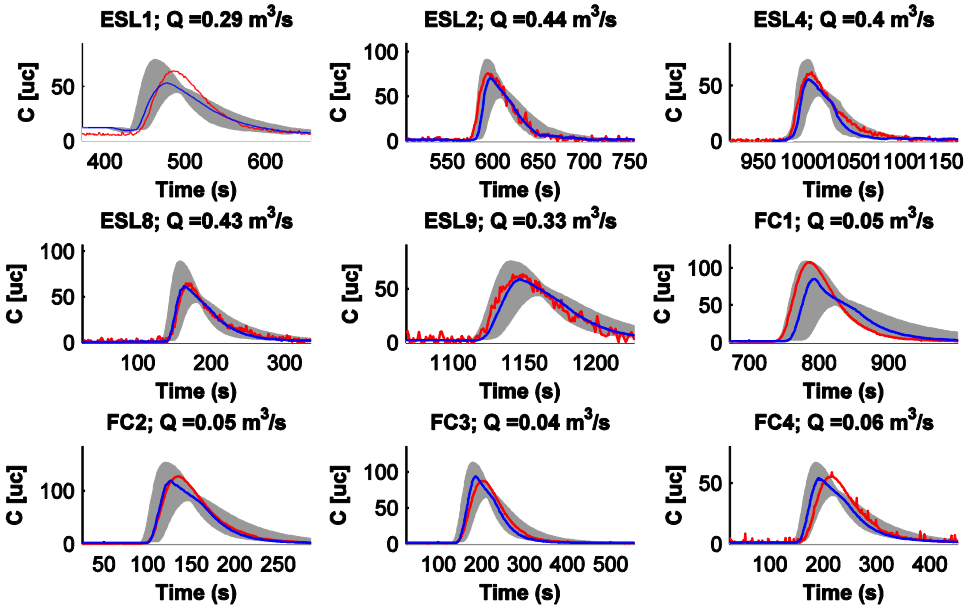

Figure 3-18. Simulated values for flow condition corresponding to campaign No 2. Red and blue lines are the observed and mean simulated breakthrough curves, respectively. The shaded area is limited by the 95th percentile and 5th percentile of predictive distributions.

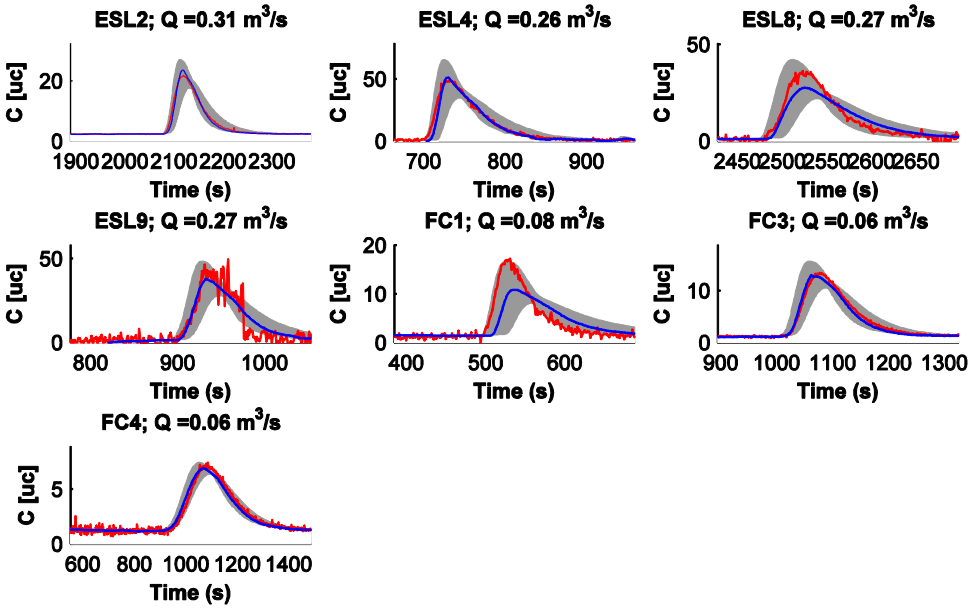

Figure 3-19. Simulated values for flow condition corresponding to campaign No 3. Red and blue lines are the observed and mean simulated breakthrough curves, respectively. The shaded area is limited by the 95th percentile and 5th percentile of predictive distributions.

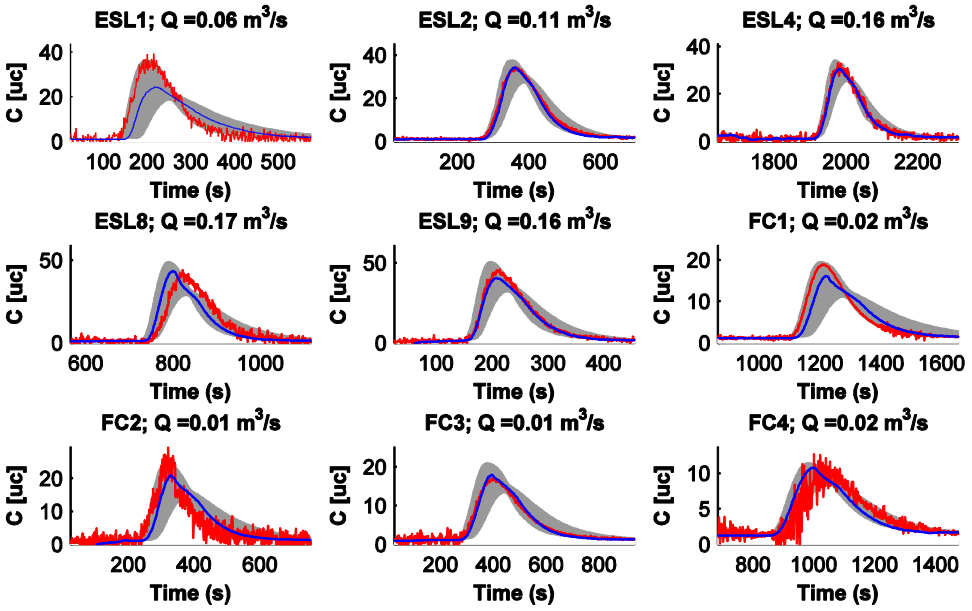

Figure 3-20. Simulated values for flow condition corresponding to campaign No 4. Red and blue lines are the observed and mean simulated breakthrough curves, respectively. The shaded area is limited by the 95th percentile and 5th percentile of predictive distributions.

Figure 3-17 to Figure 3-20 indicate that the predictions of the breakthrough curves are reasonable, taking into account that the observed values fall within the 95% prediction intervals of the model. For some cases, the model was not applied because of the poor quality of the tracer signals, which could bias the calculated efficiency. Nonetheless, the rest of the data are likely influenced by this issue to some degree. Additionally, there was no pattern that suggested a better or worse performance of the model in relation to discharge. What we found, however, was that 25 of the 31 cases had less accurate simulation at the rising portion of the breakthrough curves. This could be associated with the selection of the relationship t^*_m - q^* instead τ^* - q^* within the simulation procedure, and could also reflect the fact that the total uncertainty propagation creates a perturbation in the simulated values near the peak concentration region. This statement is illustrated in Figure 3-21, where the total uncertainty (complete shaded area) was disaggregated so that partial contributions can be identified. The clearest area represents the uncertainty contribution arising from the creation of random step-pool-run sequences. This area represents an important portion of the total shaded area. Besides, the yellow curve, which corresponds to the mean prediction for that case, has more agreement with the measured concentration signal. When uncertainty coming from estimation of the mean travel time is introduced, a second large contribution appears, causing the above-mentioned deviation of the mean prediction. The third contribution (darkest area) responds to uncertainty coming from the estimation of the dispersive fraction, which became less important for all cases.

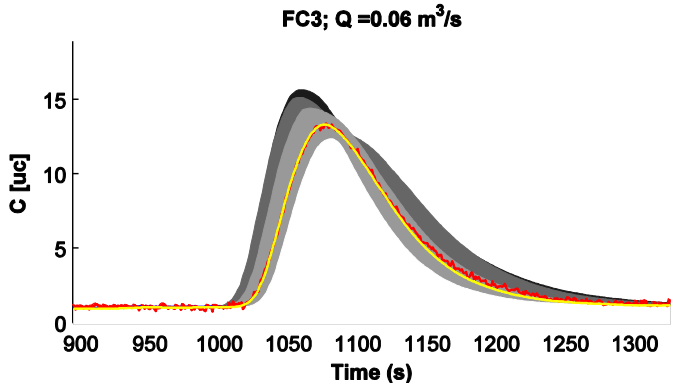

Figure 3-21. Contributions to uncertainty coming from the stochastic representation of characteristic lengths and the empirical relationships derived for estimating the mean travel time and the dispersive fraction.

3.5 CONCLUSIONS

Data from nine step-pool reaches surveyed at four different flow conditions allowed us to link stream-bed (step height, pool length and step to step length) and stream-pattern variability (coefficient of variation of width) with dispersive characteristics represented by the aggregated dead zone (ADZ) approach. The characteristic travel times, t_m (mean travel time) and τ (first arrival time), showed an invariant behavior with discharge, when these variables were normalized using the bankfull width (W_B) and the mean step height (H_s). Moreover, using step height instead of a representative sediment diameter to obtain the unit discharge, q^*, lead to an isolation of the effect of the step-forming process on the resulting scaling law. Conversely, the dispersive fraction (DF) did not show any discharge dependence, but did display high variance in relation to differences in geometry between stream reaches.

The data analyzed here indicate that solute dispersion along a step-pool channel is influenced by two separate morphological settings operating at different scales. The longitudinal arrangement of steps, pools and runs appear to explain the mean dispersive response within a reach better than discharge, thus making longitudinal morphology the explanatory variable when the spatial scale is changed, i.e., when one is interested in assessments of solute transport processes within different step-pool reaches throughout a watershed. The pool length to step-to-step length ratio (L_{pool}/L_s) is proposed to assess such spatial scale changes not only because this quantity is intuitively linked with the theoretical definition of $DF = V/V_{TOTAL}$, but also because both quantities can be probabilistically related to the reach-average bankfull width (W_B). An exponential distribution is appropriate to represent the probabilistic behavior.

Within a reach, weak evidence was found regarding the planform variability contribution on dispersion, expressed as the coefficient of variation of width. However, the increasing trend observed in the CVw vs DF diagram, and the decreasing trend of CVw with discharge, suggest a major influence from pool widths when discharge becomes lower. Taking these results into account, as well as analyses by *Zhang and Boufadel* [2010], we hypothesize that variability of pool widths explains variability of the dispersive fraction around the mean value estimated from the ratio (L_{pool}/L_{step}), a variance that we did not include in our analysis. Further work should include this degree of freedom when explaining variability of DF.

Considering that the morphological variables that we analyzed are relatively easy to estimate either by field surveys or indirect methods (downstream hydraulic geometry approaches, digital elevation models, aerial images, etc.), the morphologic and stochastic framework presented here for modeling solute transport provides a useful tool for hydrological modeling. The method is likely to be useful for solute transport applications from the reach scale to the basin scale where insufficient detailed field measurements exist.

It would be interesting to derive an enhanced scheme for which dispersion downstream could be simulated not by a lumped set $(DF, t_m, \tau)_{\text{Lumped}}$, but by the cumulative dispersion effect caused by a connected cluster of step-pool-run units, each characterized by a set of parameters $(DF, t_m, \tau)_{\text{Unit}}$. Nevertheless, we are aware that our proposed approach must first be tested in different geomorphic settings, including channels with different step-forming processes.

3.6 ACKNOWLEDGMENTS

Special thanks to the support provided by COLCIENCIAS and National University of Colombia, since they made it possible for MAJ to collaborate with EW at Colorado State University. We are very grateful to Gabrielle David and Steve Yochum, who collected the field data used here with support from NSF grant EAR-0608918, and to David Dust for providing constructive ideas regarding step-pool systems. The paper was improved by comments from four anonymous reviewers.